

## Erosion Process of Multiple Debris Flow Surges Caused by Check Dam Removal: An Experimental Study

Xi'an Wang<sup>1,2</sup> , Jiangan Chen<sup>1,2,3</sup> , Huayong Chen<sup>1,2,3</sup> , Xiaoqing Chen<sup>1,2,3</sup> , Shuai Li<sup>1,3</sup> , and Wanyu Zhao<sup>1,2,3</sup> 

<sup>1</sup>Key Laboratory of Mountain Hazards and Earth Surface Process, Institute of Mountain Hazards and Environment, Chinese Academy of Sciences, Chengdu, China, <sup>2</sup>University of Chinese Academy Sciences, Beijing, China, <sup>3</sup>China-Pakistan Joint Research Center on Earth Sciences, CAS-HEC, Islamabad, Pakistan

### Key Points:

- The evolution of the stored sediment landform and debris flow erosion efficiency were revealed
- The erosion volume development process was clarified, and its calculation formula was established
- The distribution characteristics of the erosion volume along the flume were described by the Weibull distribution

### Correspondence to:

J. Chen,  
[chenjg@imde.ac.cn](mailto:chenjg@imde.ac.cn)

### Citation:

Wang, X., Chen, J., Chen, H., Chen, X., Li, S., & Zhao, W. (2022). Erosion process of multiple debris flow surges caused by check dam removal: An experimental study. *Water Resources Research*, 58, e2021WR030688. <https://doi.org/10.1029/2021WR030688>

Received 25 JUN 2021  
Accepted 7 FEB 2022

**Abstract** Debris flows are one of the most serious natural disasters on Earth and cause great losses in human life and property each year. Check dams have been widely utilized in debris flow hazard mitigation, and over time, some control projects have exceeded their designed service lifetime. However, the processes of stored sediment erosion with multiple surges of debris flows after check dam removal are unknown. Here, the stored sediment erosion processes associated with different reductions in the dam height (i.e., the removed height) were revealed by physical experiments. The results showed that erosion was concentrated on the stored sediment scarp formed by dam removal and that the erosion process mainly included undercutting and widening. The erosion efficiency of the debris flow gradually decreased with the development of erosion and was positively correlated with removed height, negatively correlated with the accumulated debris flow volume, and proportional to the remaining potential volume of sediment to be eroded. The erosion volume development process was well described by an exponential function model, and the physical meanings of the parameters in the model and their empirical values were clarified. Moreover, the distribution of the erosion volume along the flume was shown to satisfy the Weibull distribution, and the distribution parameters were related to the removed height, erosion volume, and sediment volume fraction of the debris flow. We anticipate that our results will serve as a starting point for the demolition and reconstruction of debris flow hazard mitigation engineering in mountainous areas.

## 1. Introduction

Check dams, namely, transverse structures built across gullies, are one of the most effective methods of mitigating debris flow hazards worldwide (Abbasi et al., 2019; X. Chen et al., 2015; Galia et al., 2021; Lucas-Borja et al., 2021; Pourghasemi et al., 2020). They can not only retain debris flow materials but also block boulders carried by debris flows to separate water from stone and reduce the subsequent impact forces on housing and bridges (X. Chen et al., 2015; Piton & Recking, 2016; Z. Wang et al., 2021; X. Zhang et al., 2021). However, compared with other dams constructed with reinforced concrete, check dams are more vulnerable to failure due to their construction from loose stone and their masonry structure (X. Chen et al., 2015; J. Chen et al., 2021; Z. Chen et al., 2021; Meng, 2012; Mikoš et al., 2014). The full life cycle of a check dam faces various challenges, such as foundation scour, the impacts of large-scale debris flows, and the loss of its regulated storage capacity (Hu et al., 2020; Huang et al., 2021; S. Li et al., 2019; Pan et al., 2013). If check dams are completely broken down or partially destroyed under the action of major debris flow events, the stored sediment may transform into debris flows and cause serious sediment-related disasters downstream, even resulting river blockage and outbreak flood disasters (X. Chen et al., 2015; H. X. Chen et al., 2019; Fang et al., 2019; Liu et al., 2020; Mergili et al., 2020; Sodnik et al., 2015; Wang, 2013; White et al., 1997; Yu et al., 2013; F. Zhang et al., 2019; Zhu et al., 2013). The potential risks of check dams that reach or exceed their designed service lifetime are attracting an increasing amount of attention. Removal of the check dams can effectively release the stored sediment in the gullies, but this may cause catastrophic events. In engineering practice, partial removal and staged removal are usually used to achieve the controlled release of stored sediment (Chiu et al., 2021; H. W. Wang et al., 2014; Wang & Kuo, 2016). After the stored sediment is released, the check dams can be rebuilt, which also becomes easier with the application of prefabricated check dams such as flexible net check dams (Song et al., 2021) and steel open-type check dams (Shima et al., 2016).

© 2022. The Authors.

This is an open access article under the terms of the [Creative Commons Attribution License](https://creativecommons.org/licenses/by/4.0/), which permits use, distribution and reproduction in any medium, provided the original work is properly cited.

To date, most cases and studies of dam removal have been related to hydraulic engineering projects on rivers (Randle et al., 2015; Sawaske & Freyberg, 2012; Warrick et al., 2015), which may provide reference and comparison objects for the erosion process of debris flows and topographic changes after check dam removal. Doyle et al. (2003) investigated the evolution of the river course after the removal of two hydraulic dams and proposed that the geomorphic evolution of the channel can be divided into five stages: lowering of the water surface, incision, incision and widening, aggradation, and widening, and quasi-equilibrium. During the initial period of rapid incision, the width of the channel narrows rapidly and then enters a stage of slow widening (Cantelli et al., 2004; Ferrer-Boix et al., 2015). After incision to the base level and widening, further erosion depends on large floods (Collins et al., 2017). From the perspective of sediment transport, the process can also be divided into a transport-limited stage and a supply limited stage (East et al., 2018; Korpak & Lenar-Matyas, 2019). Factors such as grain size, levels of cohesion and consolidation, spatial variability of the deposit, deposit geometry, and removal timeline determined the rate and volume of sediment erosion (Doyle et al., 2003; Ibisate et al., 2016; Mergili et al., 2020; Sawaske & Freyberg, 2012), and an exponential function describing the evolution of the sediment erosion volume was verified based on field observation data (Collins et al., 2017; Pearson et al., 2011). Experimental studies have indicated that the sediment erosion volume depends on the removed height, water discharge, and maximum volume of sediment that can be eroded (Cantelli et al., 2004; Ferrer-Boix et al., 2015; H. W. Wang et al., 2014).

However, the characteristics of check dams are different from those of hydroelectric dams, and the material composition, movement, and erosion mechanism of debris flows are also different from those of water flows. Generally, check dams are located in gullies with steep slopes and small watershed areas, and directly confront rapid rainfall-runoff processes with a strong scouring capability and multiple surges of debris flows with large amounts of sediments, boulders, and wood fragments (X. Chen et al., 2015; H. X. Chen et al., 2019; J. Chen et al., 2020; Piton & Recking, 2016). The formation of debris flow surges is related to rainfall and the temporary storage and periodic release of sediment under specific terrains; their material composition, flow process and movement characteristics are significantly different from those of streams (N. S. Chen et al., 2011; Huebl & Kaitna, 2021; Imaizumi et al., 2019; Kean et al., 2013; Y. Li et al., 2013; Savage & Iverson, 2003; Zanuttigh & Lamberti, 2007). Therefore, the research results corresponding to the removal of hydroelectric dams cannot be simply transferred to provide guidance when removing a check dam. Previous experimental studies on the removal of check dams have mainly focused on the erosion of water flows (Chiu et al., 2021; Tseng et al., 2012). However, research on erosion processes under the action of multiple debris flow surges is lacking. The development of surges causes a significant increase in the maximum flow depth and the maximum impact pressure (Hong et al., 2015; Zanuttigh & Lamberti, 2007). In addition, the erosion effect of debris flows, as two-phase flows, is significantly different from that of water flows. The large number of solid particles in debris flows increase the fluid density and basal shear force, and the influence of particle collisions on erosion is more significant than that of water flows (Haas & Woerkom, 2016; Iverson, 2012; P. Li et al., 2020; Pudasaini, 2012; Pudasaini & Fischer, 2020; Pudasaini & Mergili, 2019). Numerical simulations based on two-phase flow (Pudasaini, 2012) or multiphase flow (Pudasaini & Mergili, 2019) models have been applied to study debris flow erosion and have achieved satisfactory results in the back calculation of glacial lake outbreak induced debris flows (Mergili et al., 2020). This method has the potential to simulate the erosion process of stored sediment under the action of debris flow surges after check dam removal, while prior to this task, the simulation method needs to be validated by field observations and experimental studies. Therefore, it is necessary to carry out experimental studies on the erosion processes of stored sediment caused by debris flow surges after removing check dams.

This research aims to investigate the influence of the removed height and the accumulated volume of debris flow surges on the erosion processes of stored sediment. To achieve this goal, we experimentally investigated three removed heights and various debris flow surges. To the best of our knowledge, this study represents the first attempt to experimentally study erosion processes of multiple debris flow surges after removing a check dam. The experimental investigation results can therefore serve as a new reference for predicting the erosion of stored sediment after breaching or removing a check dam, and the reconstruction and later management of check dams.

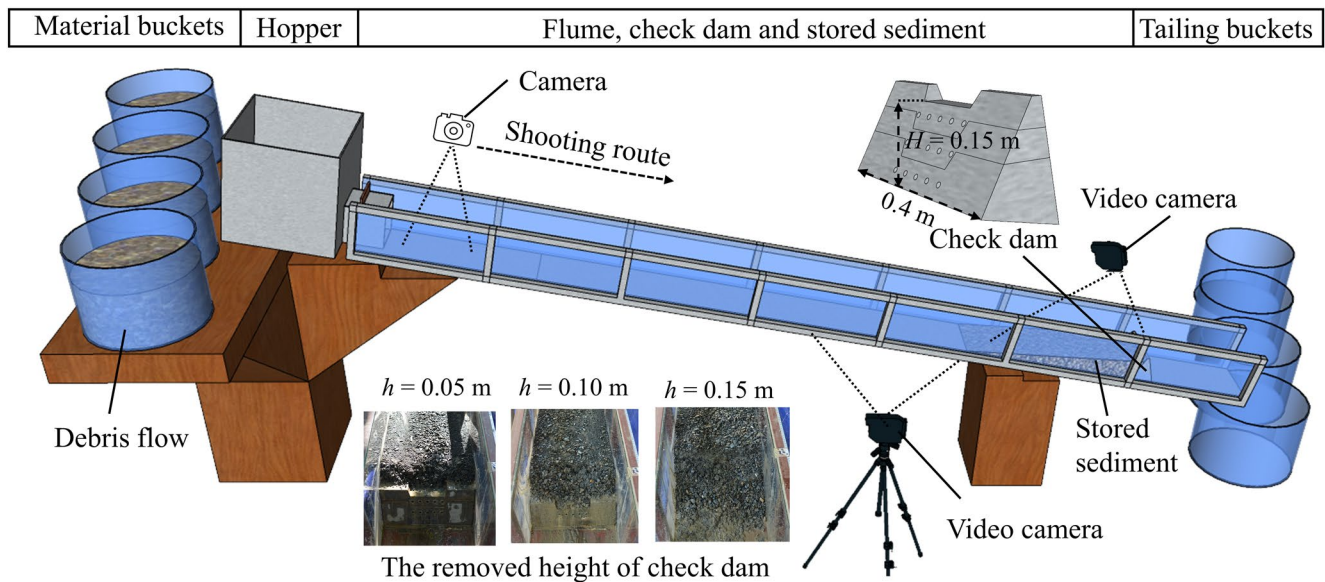


Figure 1. Experimental setup.

## 2. Materials and Methods

### 2.1. Experimental Setup

The experiments were conducted at the Dongchuan Debris Flow Observation and Research Station, Chinese Academy of Sciences, Yunnan, China. The test device consisted of material buckets, a hopper, a flume, a check dam, and tailings buckets (Figure 1). Each material bucket was used to store the mixtures of a debris flow surge. A hopper was utilized to temporarily store the mixtures, guide debris flow into the flume, and control the discharge by adjusting the opening size of the valve between the hopper and the flume. The flume measured  $7.0 \times 0.4 \times 0.4 \text{ m}^3$  (length  $\times$  width ( $B_f$ )  $\times$  height) and had a rectangular cross-section with Plexiglas installed on two sidewalls, and the slope of the test flume was 20%, which satisfied the slope range of natural debris flow gullies (N. Chen et al., 2011). The width of the check dams ( $B$ ) was 0.4 m, which was equivalent to  $B_f$ , and the height of the check dam ( $H$ ) was 0.15. The slopes of the upstream surface and the downstream surface of the check dam were 160% and 400%, respectively. The check dam consisted of three equal parts with identical heights of 0.05 m, and each part had five round drainage holes (Figure 1). The stored sediment upstream the check dam was formed by debris flow surges that were discharged from the hopper (see details in Section 2.2). Tailing buckets were placed at the end of the flume to collect the tailings of each debris flow surge.

### 2.2. Materials and Applicability

The experiments were based on a general configuration rather than a specific field case. Thus, no scaling was applied, and only some dimensionless parameters were controlled in the experiments. Each debris flow surge contained a fixed mass of granular material ( $m_s = 21 \text{ kg}$ ) and different volumes of water, and the volumes of a debris flow surge ( $V_d$ ) were  $43.9 \times 10^{-3} \text{ m}^3$  (Type 1 debris flow) and  $26.3 \times 10^{-3} \text{ m}^3$  (Type 2 debris flow). The sediment volume fraction ( $C_v = m_s / (\rho_s V_d)$ , where  $\rho_s$  is the density of sediment granules with a value of  $2,680 \text{ kg/m}^3$ ) affects the flow dynamics, erosion, and deposition of debris flows (de Haas et al., 2015; Haas & Woerkom, 2016; Pudasaini & Mergili, 2019). The  $C_v$  values of field cases are in an extremely wide range from 0.18 to 0.80 (Church & Jakob, 2020; Iverson, 1997). The debris flows in this study were selected with  $C_v$  values of 0.18 (Type 1 debris flow) and 0.30 (Type 2 debris flow), which belong to the low viscosity debris flow ( $C_v = 0.17\text{--}0.33$ ; Kang et al., 2004), and the rheological parameters of debris flow slurry can be estimated by particle size distribution (Coussot & Piau, 1994; Mooney, 1951; Yang et al., 2013). The main reason for choosing debris flows with small  $C_v$  values is that the dissipation of pore pressure in their deposits (stored sediment) is fast, which contributed to the rapid stability of the deposits and the subsequent scour experiments with multiple debris-flow surges. The Froude number ( $Fr$ ) was considered because debris flow is a gravitational process with

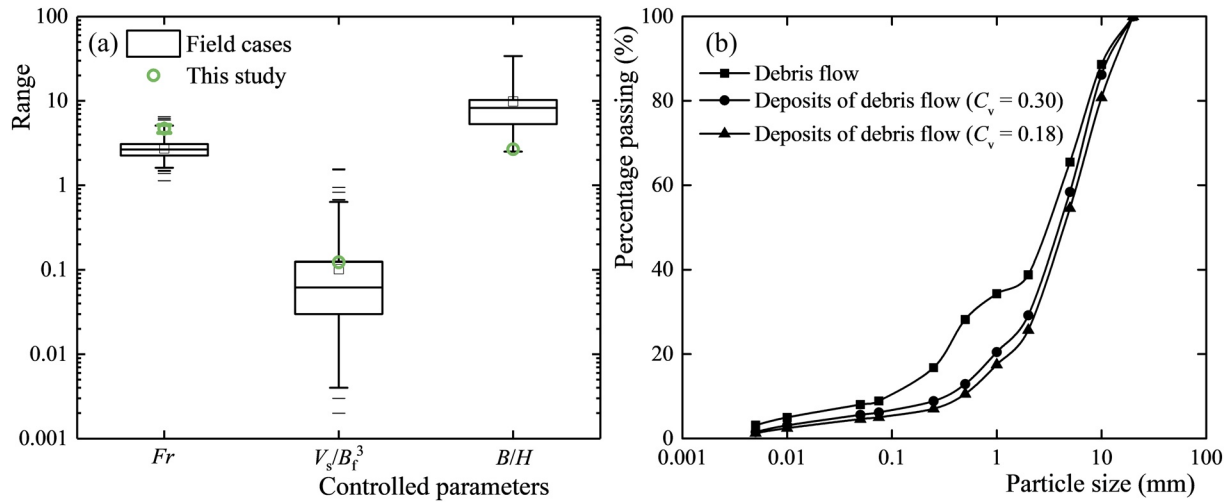


**Figure 2.** Controlled parameters of check dams, debris flow surges, and stored sediment.

open channel flow characteristics (S. Li et al., 2019; Rickenmann, 1999; Zhou et al., 2019). The  $Fr$  of a debris flow is much more complex than that of a classic single-phase flow (Iverson, 2015; Pudasaini & Kröner, 2008). We cited the previous research results and the calculation method of  $Fr$  (Choi et al., 2015):

$$Fr = \frac{v}{\sqrt{gh_d \cos \theta}} \quad (1)$$

where  $\theta$  is the channel inclination ( $^\circ$ ),  $\tan(\theta) = 20\%$ ,  $v$  is the flow velocity (m/s),  $g$  is the gravitational acceleration,  $g = 9.8 \text{ m/s}^2$ ,  $h_d$  is the flow depth (m). The values of  $v$  and  $h_d$  were measured in the experiments, and the specific method is detailed in Section 2.3. The mean value of  $Fr$  for the debris flow surges in this study was 4.68, and the standard deviation was 0.50, which is higher than the  $Fr$  in most field cases (Figure 2a), to imitate the most dangerous conditions. The field cases included 777 debris flow surges in Jiangjia gully (Kang et al., 2007; Zhang & Xiong, 1997). Moreover, the influence of the debris flow volume on the experiment had to be considered (Choi et al., 2015; de Haas et al., 2015).  $V_d$  and  $B_f$  have the following relationship:

$$V_d = vt \cdot B_f h_d \quad (2)$$

where  $t$  is the flow time (s) and the other parameters have the same meaning as previously mentioned. Dividing both sides of Equation 2 by  $B_f^3$  yields the following:

$$V_d/B_f^3 = (vt/B_f)(h_d/B_f) \quad (3)$$

Debris flow surges are characterized by a short duration, mostly  $t < 2 \text{ min}$  (N. S. Chen et al., 2011; Kean et al., 2013). When  $V_d$  increases,  $v$  and  $h_d$  increase in most debris flow events (Hong et al., 2015; Zanuttigh & Lamberti, 2007), the erosion ability of the debris flow increases, the channel erodes and widens, and  $B_f$  increases. When  $V_d$  decreases,  $v$  and  $h_d$  decrease, the debris flow deposits or even stops or changes into a water flow (de Haas et al., 2015; Iverson, 2012; Pudasaini & Fischer, 2020). Therefore, we postulated that  $V_d/B_f^3$  is constrained within a certain range under natural conditions and that  $B_f^3$  is an appropriate volume scale in this study. We constructed the dimensionless parameter  $V_s/B_f^3$  to constrain the volume of the debris flow in the experiments, where  $V_s$  is the sediment volume of a debris flow surge ( $V_s = C_v V_d$ ). According to field observation data from 777 debris flow surges in Jiangjia gully (Kang et al., 2007; Zhang & Xiong, 1997), the debris flow volume was reasonable in this study ( $V_s/B_f^3 = 0.122$ ; Figure 2a). Moreover, the aspect ratio ( $B/H$ ) of the check dam model was consistent with the aspect ratios of actual projects with 30 debris flow check dams in the Minjiang River Basin (Figure 2a).

Figure 2b shows the grain-size distribution of the granular material of debris flow and stored sediment. The granular material for the tests was obtained from the debris flow deposition fan of Jiangjia gully. Granular material with a diameter larger than 20 mm was removed to allow the debris flow to travel smoothly through the

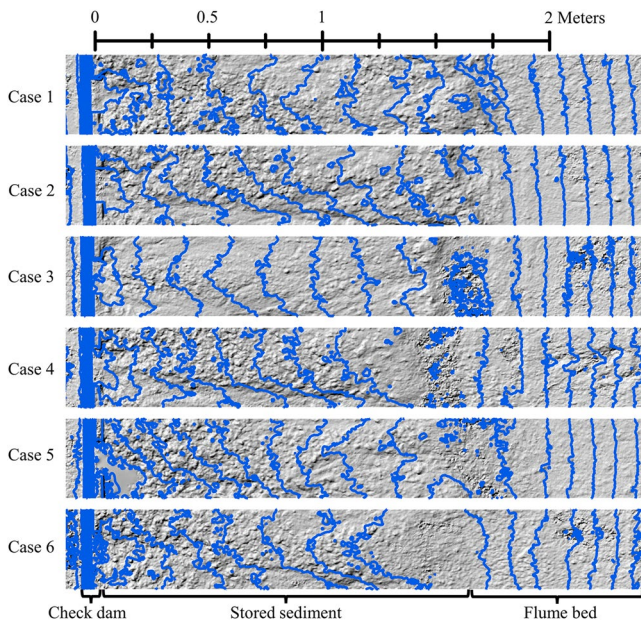


**Figure 3.** Topographic map of deposits upstream of check dams (vertical interval: 0.02 m).

flume. This design has also been employed in other experiments (X. Chen et al., 2017; J. Chen et al., 2018; Cui et al., 2015; S. Li et al., 2019).

Before the start of the test (before removal), 10 debris flow surges were regulated by the check dam to form stored sediment. Water and some fine particles were discharged downstream through the overflow and drainage holes of the check dam. Therefore, the fine particle content of stored sediment is smaller than that of debris flow (Figure 2b). The landform characteristics of stored sediment are shown in Figure 3. The dry densities ( $\rho_d$ ) of stored sediment formed by the Type 1 debris flow and Type 2 debris flow were measured by the ring knife method, and were approximately 1,786 and 1,975 kg/m<sup>3</sup>, respectively. It should be noted that the dry density measurement was carried out in additional experiments because ring knife sampling destroyed the stored sediment and would affect the subsequent erosion experiments. Based on the grain-size distribution and  $\rho_d$ , the saturated hydraulic conductivity of the stored sediment can also be evaluated according to the empirical formulas (Chapuis, 2004). The removal of the check dam was started when there was no obvious seepage discharge through the drainage holes of the check dam (approximately 4 min after the debris flow passed), and pictures of stored sediment after check dam removal are shown in Figure 1.

### 2.3. Repetitions and Measured Variables

This study included six experiments, and Table 1 shows the control parameters for each experiment, in which  $V_{init}$  and  $L_{init}$  are the volume and length of the stored sediment, respectively,  $N$  is the cumulative number of debris flow surges, the other parameters have the same meaning as previously mentioned. After check dam removal, four debris flow surges eroded the stored sediment for all cases, and the time interval between adjacent surges was 4 min. To simulate a debris flow surge, the mixtures of a debris flow surge were first transferred from the material bucket to the hopper, and the mixtures were released to the flume by opening the valve at the bottom of the hopper. After each debris flow surge, the cumulative number of surges was counted as  $N$  (Table 1). The morphological characteristics of the stored sediment were recorded by a camera (Nikon D850, 6,016 × 4,016 pixels,  $f = 24$  mm; Figure 1), and digital elevation models (DEMs) were obtained based on photogrammetry (Qin et al., 2018). The volume ( $V_{ero}$ ) and distribution of eroded sediment were obtained by a comparison of repeat DEMs (DEMs of difference; Cucchiario et al., 2019). A video camera (GoPro hero7 Black, 4,096 × 2,160 pixels, 25 fps) installed on the top of the flume recorded the erosion process. With large tracer particles, a video camera (SONY FDR-AX60, 4,096 × 2,160 pixels, 25 fps) on the side of the flume recorded the velocity ( $v$ ) and depth ( $h_d$ ) of the debris flow before it entered the check dam.

### 2.4. Parameters and Dimensional Analyses

Various parameters were considered in this study. These parameters were classified into controlled parameters and measured parameters, and a series of dimensionless parameters (derived variables) were constructed based on previous studies and the needs of this study, which facilitated the display and discussion of the test results. The control parameters are summarized as follows:

$B$  is the width of the check dam (m);  $B_f$  is the width of the flume (m);  $C_v$  is the sediment volume fraction of debris flow (–);  $Fr$  is the Froude number of debris flow;  $g$  is the gravitational acceleration,  $g = 9.8$  m/s<sup>2</sup>;  $h$  is the removed height of the check dam (m);  $H$  is the initial effective height of the check dam (m);  $N$  is the cumulative number of debris flow surges (e.g., 1, 2, 3, 4; –);  $V_d$  is the volume of a debris flow surge (m<sup>3</sup>), and is the derivative of  $V_d$  ( $V_d = \Delta V_D$ );

**Table 1**  
Experimental Arrangement and Test Conditions

| Case   | Removed height $h$ (m) | Stored sediment |                                                | Debris flow |     |           |
|--------|------------------------|-----------------|------------------------------------------------|-------------|-----|-----------|
|        |                        | $L_{init}$ (m)  | $V_{init}$ ( $\times 10^{-3}$ m <sup>3</sup> ) | $C_v$       | $N$ | $Fr$      |
| Case 1 | 0.15                   | 1.88            | 85.4                                           | 0.18        | 1–4 | 4.13–5.52 |
| Case 2 | 0.10                   | 1.78            | 79.4                                           | 0.18        | 1–4 | 4.04–4.39 |
| Case 3 | 0.05                   | 1.78            | 82.3                                           | 0.18        | 1–4 | 4.21–5.52 |
| Case 4 | 0.15                   | 1.77            | 74.4                                           | 0.30        | 1–4 | 4.05–4.96 |
| Case 5 | 0.10                   | 1.79            | 79.0                                           | 0.30        | 1–4 | 4.34–5.39 |
| Case 6 | 0.05                   | 1.71            | 73.5                                           | 0.30        | 1–4 | 4.13–5.39 |

$V_D$  is the accumulated volume of the debris flow surges ( $m^3$ ),  $V_D = \int Q \cdot dt$ , where  $Q$  is the discharge of debris flow ( $m^3/s$ ), and  $t$  is time (s). When accumulating  $N$  debris flow surges,  $V_D = NV_d$ .

The measured parameters are summarized as follows:

$h_d$  is the flow depth (m);  $L$  is the horizontal distance between any point of stored sediment and the check dam (m);  $L_{init}$  is the horizontal initial length of stored sediment (m);  $v$  is the flow velocity (m/s);  $V_{ero,i}$  is the volume of sediment eroded by the  $i$ -th debris flow surge ( $m^3$ );  $V_{ero}$  is the accumulated volume of sediment eroded by debris flow surges ( $m^3$ );  $V_{init}$  is the initial stored sediment volume ( $m^3$ ).

This study focused on constructing dimensionless parameters that served as a convenient reference in engineering practices.

$\lambda = \frac{V_{ero}}{V_{init}}$ , the erosion volume ratio. It was used to describe the development process of erosion volume and similar parameters were employed by Sawaske and Freyberg (2012) and Ferrer-Boix et al. (2015). In this study, after  $N$  debris flow surges, the calculation method was  $\lambda = \sum_{i=1}^N \frac{V_{ero,i}}{V_{init}}$ .

$\zeta = \frac{\partial V_{ero}}{\partial V_D}$ , the erosion efficiency of debris flow, and similar parameters were utilized by Sawaske and Freyberg (2012). However, the fully mechanics-based erosion rate models presented by Pudasaini and Fischer (2020) and Pudasaini and Krautblatter (2021) can physically much better simulate the erosion and mass transport processes of natural events. The physical meaning of  $\zeta$  is the ratio of the volume of erosion to the debris flow volume entering the study area per unit time ( $\Delta t$ ),  $\zeta = \frac{\bar{E}\Delta t S}{Q\Delta t} = \frac{\bar{E}S}{Q}$ , where  $\bar{E}$  is the average erosion rate in the study area (m/s),  $S$  is the study area ( $m^2$ ), and  $Q$  is the discharge of debris flow entering the study area ( $m^3/s$ ). In this study, for the  $i$ -th debris flow surge, the erosion efficiency was calculated by  $\zeta_i = V_{ero,i}/V_d$ .

$h_* = h/H$  is the removed height ratio of check dam.

$V_* = V_D/B_f^3$ , the relative accumulated volume of the debris flow eroding the stored sediment (where  $B_f^3$  is the volume scale in this study), and a similar parameter was applied by Ferrer-Boix et al. (2015). In this study, after  $N$  debris flow surges, the calculation method was  $V_* = NV_d/B_f^3$ .

$V_{pote} = (h_*^2 V_{init} - V_{ero})/B_f^3$  represents the relative remaining potential volume of sediment to be eroded, where  $B_f^3$  is the volume scale in this study. The longitudinal section of the stored sediment could be approximately regarded as a triangle (Figure 1). We assumed that the base level of erosion after dam removal is parallel to the original gully bed (flume bed). When the removed height ratio was  $h_*$ , the maximum potential volume of sediment to be eroded is  $h_*^2 V_{init}$ . In this study, for the  $N$ -th debris flow surge, the average relative remaining potential volume was calculated by  $V_{pote,N} = \left( h_*^2 V_{init} - \sum_{i=1}^{N-1} V_{ero,i} - 0.5V_{ero,N} \right) / B_f^3$ .

$y = L/L_{init}$  represents the longitudinal section coordinates taking the upstream edge of the check dam as the coordinate origin and taking  $L_{init}$  as the unit length and the upstream horizontal direction to be positive direction.

### 3. Results

#### 3.1. Erosion Process

After check dam removal, a scarp formed downstream of the stored sediment (Figure 4c), and the main erosion was concentrated here. The main forms of erosion were headward and lateral erosion, and the erosion process was divided into 4 stages, as shown in Figure 4:

1. Headward erosion initiation: the demolition of the check dam caused the formation of a nick point (scarp) at the original dam site. Because the scarp increased the bed slope and weakened the resistance of the gully bed, erosion quickly started and developed upstream under the action of the debris flow (Figure 4b). In addition, due to the differences in flow conditions and the sediment texture on the cross section, the headward erosion exhibited differences in the cross section. The differential erosion advanced the erosion process to the second stage.
2. Incision and rill formation: the headward erosion length differed at different points of the cross section due to differential erosion, which produced obvious rills on the stored sediment (Figure 4c). The rills aggravated the

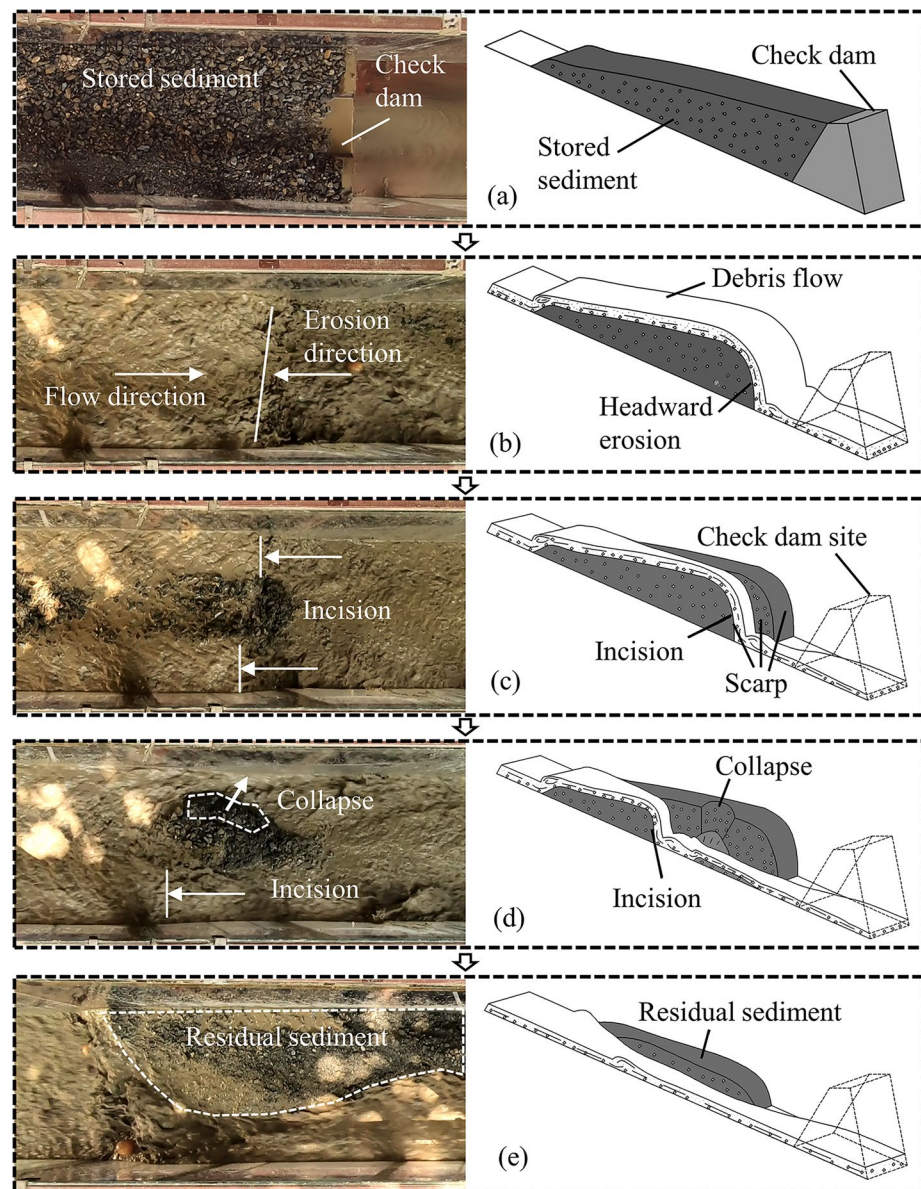


**Figure 4.** Erosion process of stored sediment after check dam removal (Case 1).

flow condition differences in the cross section, and subsequent debris flows preferentially passed along the rills, which strengthened the headward erosion at the upstream end of the rills. These resulted in the further development of the rills.

3. Lateral erosion and widening: with the development of rill length and depth, the sediment on both sides of the rills gradually became unstable due to the removal of lateral constraint, and supplied material to the rills through the instability of the slope (Figure 4d). The subsequent debris flow eroded and transported these materials and increased the instability of the slopes on both sides. These processes gradually increased the width of the rills. The test revealed that periodic slope instability was the main form of lateral erosion. The entrainment and seepage of debris flows may be controlling factors because they needed enough time to accumulate their influence, promoting slope instability, and then needed to reaccumulate their influence after slope instability. Entrainment tended to shape the rill sidewall into a high and steep slope (Figure 4d) to provide topographical conditions for slope instability. Seepage increased the water content of the sidewall and reduced the effective stress and internal friction angle of the stored sediment to provide mechanical conditions for slope instability.

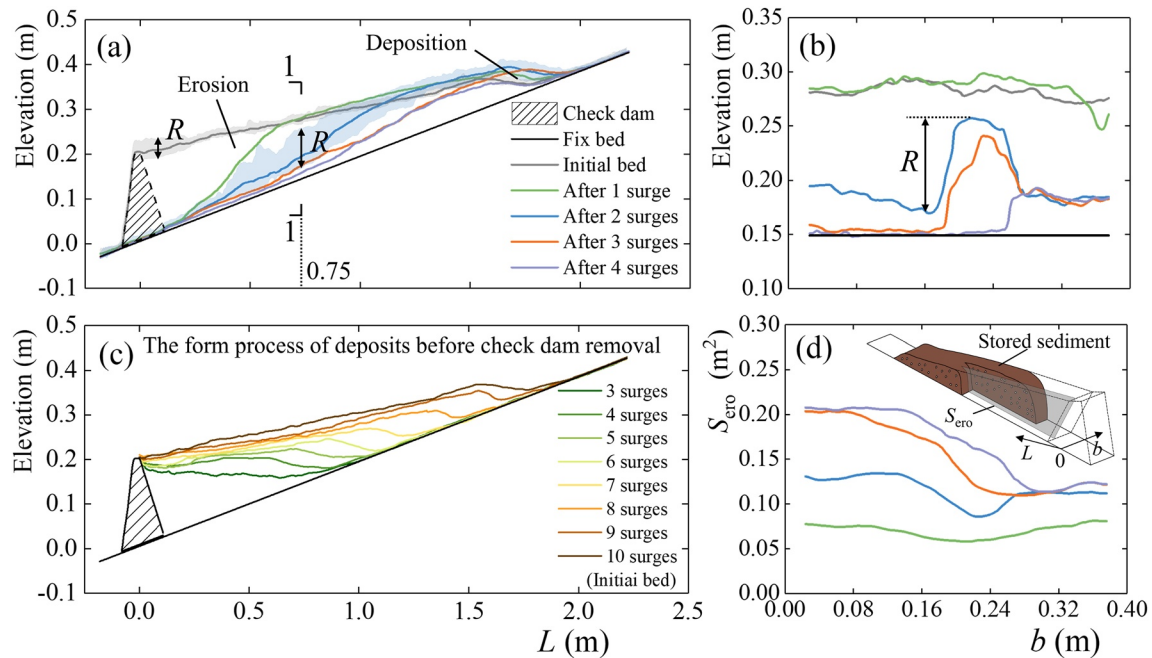


Figure 5. Erosion and deposition characteristics of stored sediment (Case 1).

4. Quasi-equilibrium formation stage: the depth, width and length of the rills gradually increased until they became largely stable after multiple debris flow surges; a quasi-equilibrium state was gradually reached when the debris flow scale stabilized (Figure 4e).

Figure 5 describes the erosion characteristics of the stored sediment by using Case 1 as an example. Figures 5a and 5c show the evolution characteristics of the longitudinal section in the erosion phase after dam removal and the deposition phase before dam removal, respectively. Figures 5b and 5d show the evolution characteristics of a single cross section (Section 1-1 in Figure 5a) and the distribution characteristics of erosion along the cross section, respectively. In the figure,  $b$  is the distance between any point of the stored sediment and the right side-wall of the flume (m),  $S_{\text{ero}}$  is the sediment erosion area on every longitudinal section ( $\text{m}^2$ ),  $R$  is the topographic relief of the cross section (m), the solid lines in Figures 5a and 5c represent the average elevation, and the shaded part is the elevation range.

The erosion of stored sediment had the characteristics of typical headward erosion. The eroded volume of stored sediment gradually increased with the accumulative action of the debris flow surge; however, the eroded volume of each surge gradually decreased (Figure 4a). Moreover, the erosion depth exhibited obvious differences in the cross section, and sediment erosion preferentially started from one side (or both sides) and then developed to the other side (or middle; Figure 5b). The erosion difference of each surge in the cross section first increased and then decreased with an increase in debris flow surges (Figure 5d).

Figure 5a also shows sediment siltation upstream of the deposit, which is the result of incomplete deposition upstream of the check dam due to the limited number of surges in the deposition phase, as shown in Figure 5c. As the number of debris flow surges increased, sediment siltation gradually decreased until eventually ceasing (Figure 5a), which is the result of headward erosion and rill development. The formed rills optimized the flow cross section of the debris flow and promoted the smoother passage of the debris flow through the stored sediment. Therefore, the volume of new siltation gradually decreased after dam removal. In addition, because the volume of the new siltation was small, its influence was not considered in subsequent studies.

### 3.2. Evolution of the Erosion Volume

The evolution of the erosion volume could describe the erosion macroscopically. Figure 6a shows that the erosion efficiency ( $\zeta$ ) was positively correlated with the removed height ratio ( $h_*$ ). With an increase in  $h_*$ , the length and

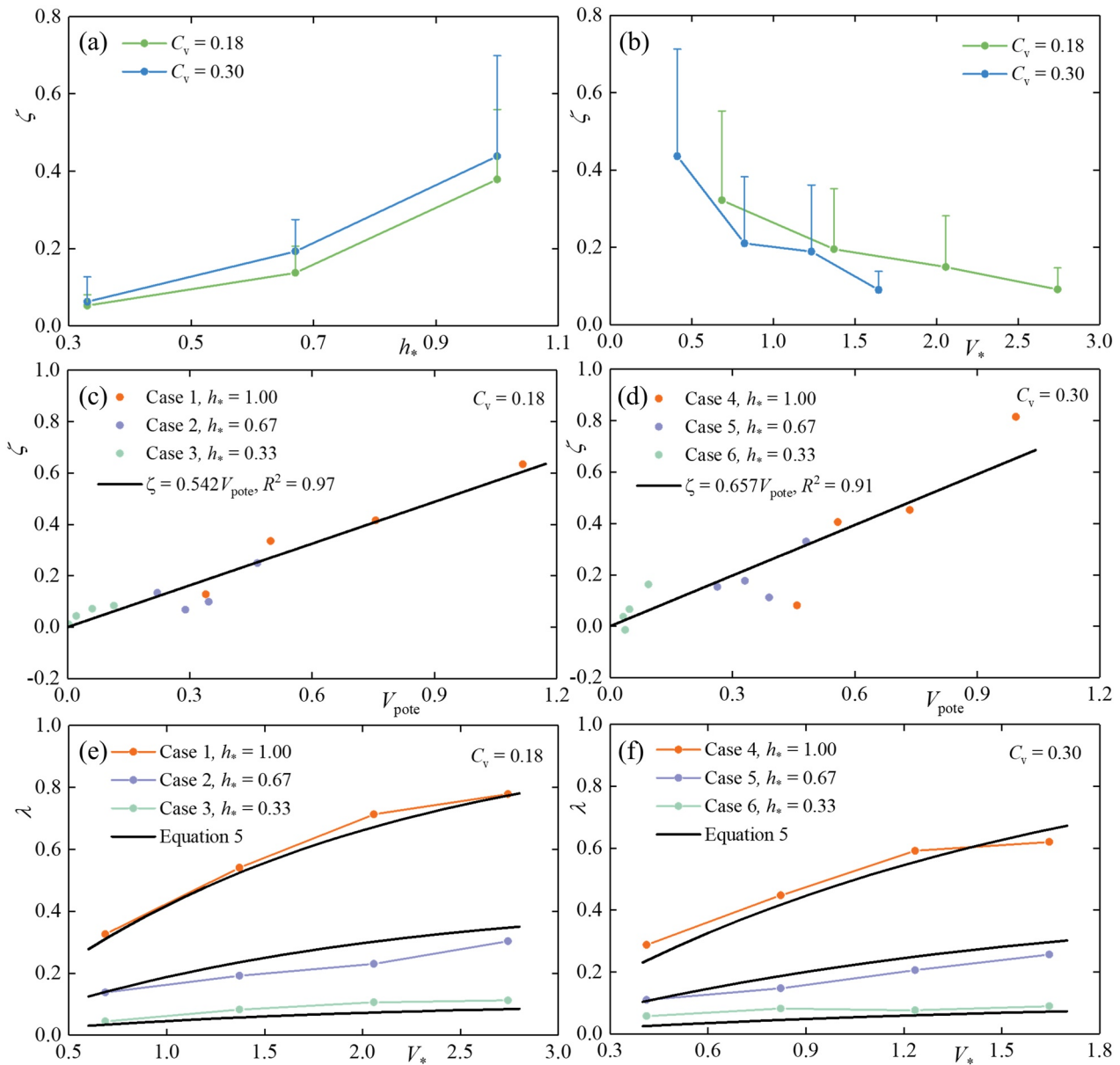


Figure 6. Erosion efficiency of the debris flow and the erosion volume ratio of stored sediment.

slope of the scarp downstream of the stored sediment increased (Figure 4c). For headward erosion, an increase in the slope would weaken the resistance of the gully bed, promoting an increase in the erosion rate, and an increase in the length of the scarp would increase the area of headward erosion and promote an increase in the erosion volume. In addition, higher scarp was more likely to lose stability and increased the volume of erosion under the action of lateral erosion. Figure 6a also shows that the debris flow with  $C_v = 0.30$  generally had a higher  $\zeta$  than the debris flow with  $C_v = 0.18$ , which was mainly attributed to an increase in the basal shear stress and collision stress of the debris flow with an increase in  $C_v$ .

Figure 6b shows that  $\zeta$  was negatively correlated with the relative accumulated volume of the debris flow ( $V_*$ ). With an increase in  $V_*$ , erosion gradually developed upstream, the thickness of the stored sediment gradually decreased (Figure 5a), and the height of the scarp (Figure 4c) decreased. The erosion volume of a surge decreased for the same reason as mentioned in the above paragraph. The abovementioned analysis also shows that the erosion process of stored sediment after check dam removal was a negative feedback process. With the

development of erosion,  $\zeta$  was gradually suppressed. A mathematical model reflecting the negative feedback process was constructed below.

Figures 6c and 6d show that the relative remaining potential volume of sediment to be eroded ( $V_{pote}$ ) had a significant impact on  $\zeta$  and  $\zeta$  was proportional to  $V_{pote}$ :

$$\zeta = kV_{pote} \quad (4a)$$

where  $k$  is the proportional coefficient with values of 0.542 and 0.657 for  $C_v = 0.18$  and 0.30, respectively. The physical meaning of  $\zeta$  is expressed as follows (more details in Section 2.4):

$$\zeta = \frac{\partial V_{ero}}{\partial V_D} \quad (4b)$$

Substituting  $V_{ero} = \lambda V_{init}$  and  $V_D = B_f^3 V_*$  (Section 2.4) into Equation 4b and combining Equation 4a and Equation 4b yields the following:

$$\frac{V_{init} \partial \lambda}{B_f^3 \partial V_*} = kV_{pote} \quad (4c)$$

Substituting  $V_{pote} = V_{init} (h_*^2 - \lambda) / B_f^3$  (Section 2.4) into Equation 4c yields the following:

$$\frac{\partial \lambda}{\partial V_*} = k (h_*^2 - \lambda) \quad (4d)$$

The differential equation (Equation 4d) was solved:

$$\lambda = h_*^2 (1 - \exp(-kV_*)) \quad (4e)$$

Equation 4e shows that as  $V_*$  increased,  $\lambda$  gradually approached the constant  $h_*^2$ , and  $h_*^2 V_{init}$  represented the maximum potential volume of stored sediment that could be eroded.  $k$  is the proportional coefficient indicating the relationship between  $\zeta$  and  $\lambda$ . However, these empirical equations cannot explain the real physical process of erosion. To appropriately describe the erosion and entrainment processes and the associated mass flow mobility, we must use the mechanical erosion models developed by Pudasaini and Krautblatter (2021). This research provides empirical values of  $k$  through physical experiments. Substituting the value of  $k$  in Figures 6c and 6d into Equation 4e, the calculation formula of  $\lambda$  can be obtained:

$$\lambda = \begin{cases} h_*^2 (1 - \exp(-0.542V_*)) & C_v = 0.18 \\ h_*^2 (1 - \exp(-0.657V_*)) & C_v = 0.30 \end{cases} \quad (5)$$

Figures 6e and 6f show the comparison between the calculated and measured values of  $\lambda$ . The comparison result shows that the error between the calculated value and the measured value was small, which indicated that Equation 5 described the evolution of the erosion volume very well and that the assumption of the maximum potential volume of stored sediment to be eroded ( $h_*^2 V_{init}$ ) was reasonable. These results provided a reference for the engineering removal of check dams, especially the removed height and erosion disasters after check dam removal or failure. In addition, these results also provided a simple method to evaluate the erosion processes of stored sediment. For example, when only limited  $\zeta$  data are observed, this method could aid in evaluating and predicting the overall erosion process.

### 3.3. Longitudinal Distribution of the Eroded Sediment

To further study the longitudinal spatial distribution characteristics of the eroded sediment, we analyzed the influence of  $h_*$  and  $\lambda$  on the probability distribution of longitudinal position  $Y$  of eroded sediment. The results showed that  $Y$  obeyed the Weibull distribution; its probability density function is expressed as follows:

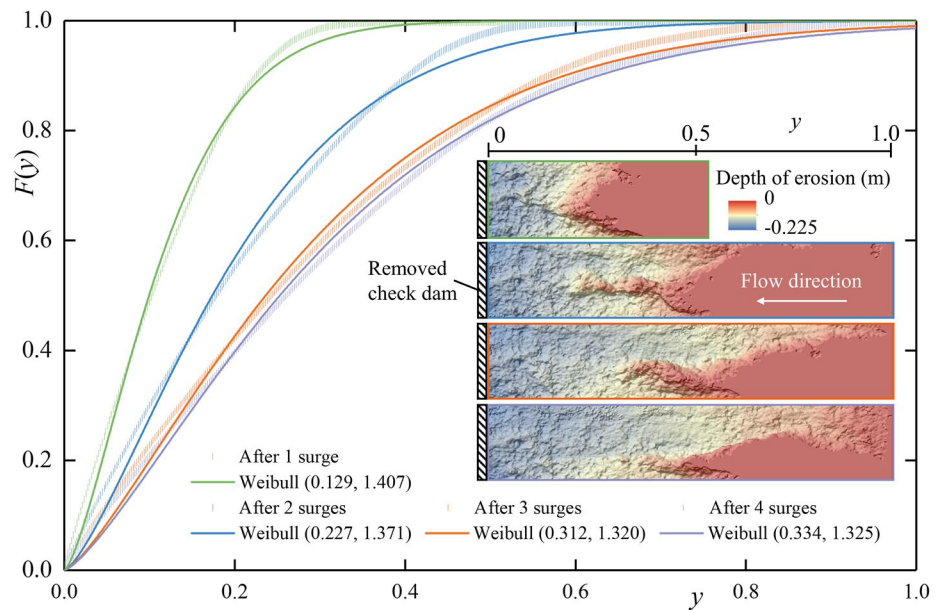


Figure 7. Cumulative curves of the longitudinal position of eroded sediment after different debris flow surges in Case 1.

$$f(y|\eta, \beta) = \begin{cases} \frac{\beta}{\eta} \left(\frac{y}{\eta}\right)^{\beta-1} \exp\left(-\left(\frac{y}{\eta}\right)^\beta\right), & y > 0 \\ 0, & y \leq 0 \end{cases} \quad (6)$$

Its cumulative probability is more convenient for use:

$$F(y) = 1 - \exp\left(-\left(\frac{y}{\eta}\right)^\beta\right) \quad (7)$$

Table 2  
Scale Parameters and Shape Parameters Under Various Test Conditions

| $h_*$ | $N$ | $C_v = 0.18$ |        |         |       | $C_v = 0.30$ |        |         |       |
|-------|-----|--------------|--------|---------|-------|--------------|--------|---------|-------|
|       |     | $\lambda$    | $\eta$ | $\beta$ | $R^2$ | $\lambda$    | $\eta$ | $\beta$ | $R^2$ |
| 1.00  | 1   | 0.326        | 0.129  | 1.407   | 0.997 | 0.288        | 0.120  | 1.236   | 0.999 |
| 1.00  | 2   | 0.540        | 0.227  | 1.371   | 0.995 | 0.448        | 0.216  | 1.209   | 0.996 |
| 1.00  | 3   | 0.713        | 0.312  | 1.320   | 0.997 | 0.592        | 0.303  | 1.206   | 0.989 |
| 1.00  | 4   | 0.778        | 0.334  | 1.325   | 0.997 | 0.620        | 0.308  | 1.177   | 0.990 |
| 0.67  | 1   | 0.138        | 0.131  | 1.175   | 0.998 | 0.110        | 0.111  | 1.280   | 0.998 |
| 0.67  | 2   | 0.192        | 0.167  | 1.221   | 0.998 | 0.147        | 0.168  | 1.218   | 0.998 |
| 0.67  | 3   | 0.230        | 0.218  | 1.255   | 0.994 | 0.206        | 0.237  | 1.291   | 0.988 |
| 0.67  | 4   | 0.303        | 0.261  | 1.286   | 0.995 | 0.257        | 0.276  | 1.311   | 0.991 |
| 0.33  | 1   | 0.045        | 0.080  | 1.094   | 0.995 | 0.058        | 0.099  | 0.987   | 0.996 |
| 0.33  | 2   | 0.083        | 0.145  | 1.175   | 0.999 | 0.082        | 0.141  | 1.001   | 0.999 |
| 0.33  | 3   | 0.106        | 0.198  | 1.236   | 0.997 | 0.076        | 0.139  | 1.032   | 0.999 |
| 0.33  | 4   | 0.112        | 0.196  | 1.223   | 0.997 | 0.089        | 0.158  | 1.145   | 0.998 |
| Mean  |     |              | 0.200  | 1.257   |       |              | 0.190  | 1.174   |       |
| CV    |     |              | 0.364  | 0.068   |       |              | 0.382  | 0.091   |       |

Note. CV, coefficient of variation.

where  $\eta$  is the scale parameter and  $\beta$  is the shape parameter.

Figure 7 shows the cumulative curves of the longitudinal position of eroded sediment after the different debris flow surges in Case 1. Table 2 presents the scale parameters and shape parameters under various test conditions.  $\eta$  was positively correlated with  $\lambda$ , negatively correlated with  $h_*$ , and had the following quantitative relationship:

$$\eta = \begin{cases} 0.417 \cdot h_*^{-1.055} \cdot \lambda^{0.853}, & R^2 = 0.93 \quad C_v = 0.18 \\ 0.472 \cdot h_*^{-0.905} \cdot \lambda^{0.833}, & R^2 = 0.82 \quad C_v = 0.30 \end{cases} \quad (8)$$

When  $C_v = 0.18$  and  $0.30$ , the average values of  $\beta$  were 1.257 and 1.174, respectively, and the coefficients of variation were very small, 0.068 and 0.091, respectively. The influence of  $C_v$  on  $\beta$  was not significant, while that of  $h_*$  on  $\beta$  was significant; the two-tailed  $p$  values in Student's  $t$ -test were 0.057 ( $>0.05$ ) and 0.002 ( $<0.05$ ), respectively. The correlation between  $\lambda$  and  $\beta$  was minimal, and the correlation coefficient  $r = 0.53 < 0.6$ . These findings indicate that the longitudinal position probability distribution of eroded sediment can serve as an effective indicator for an erosion system. For example, in the case of incomplete erosion data, this distribution can aid in the reconstruction of the original erosion condition.

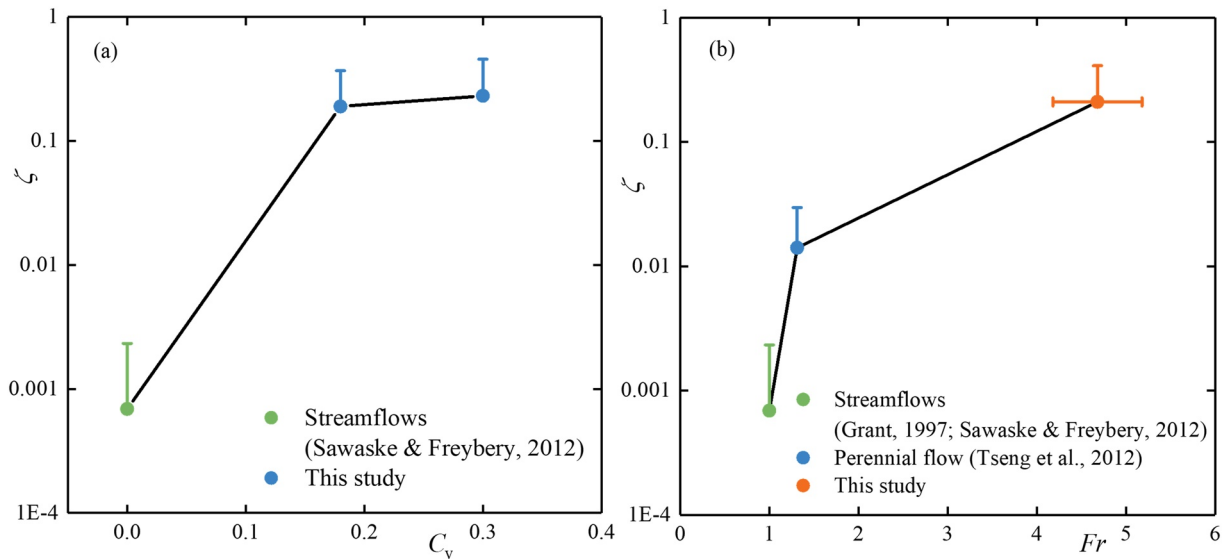


Figure 8. Comparison of  $\zeta$  of this study with those of previous studies.

#### 4. Discussion

The goal of this study was to reveal the influence of the removed height of the check dam and accumulated volume of debris flow on the erosion processes of stored sediment. The results may provide a reference for the removal of aging check dams and help avoid the rapid erosion and related disasters caused by large-scale debris flows. The removal of check dams formed a scarp downstream of the stored sediment, where the main erosion was concentrated. This study revealed that  $\zeta$  was positively correlated with  $h_*$ , negatively correlated with  $V_*$ , and proportional to  $V_{\text{pote}}$ . This study also proposed a simple calculation formula for  $\lambda$  with a clear physical meaning (Equations 4 and 5) and revealed the characteristics of the longitudinal distribution of eroded sediment.

After the removal of check dams, the evolution of the stored sediment landform mainly included two forms of incision and widening, and was controlled by headward and lateral erosion, which was similar to the evolution of the river course after hydroelectric dam removal (Cantelli et al., 2004; Doyle et al., 2003; Ferrer-Boix et al., 2015; Major et al., 2008). However,  $\zeta$  of debris flows was much greater than that of water flows, which may be caused by the difference in  $C_v$  and  $Fr$  (Figure 8). Figure 8a shows that  $\zeta$  increased with an increase in  $C_v$ . This phenomenon was attributed to the notion that the increase in  $C_v$  enhanced the base shear stress of debris flow and the collision stress of particles (Haas & Woerkom, 2016), which promoted an increase in the debris flow erosion rate according to the erosion model (Iverson, 2012), and especially with the mechanical erosion rate models (Pudasaini & Fischer, 2020; Pudasaini & Krautblatter, 2021), thereby increasing  $\zeta$ . Figure 8b shows that  $\zeta$  increased with an increase in  $Fr$  because with an increase in  $Fr$ , the velocity of the debris flow increased, the kinetic energy increased, and the erosion rate and  $\zeta$  increased when the unit discharge of the debris flow was unchanged (Fraccarollo & Capart, 2002; Mergili et al., 2017). Theoretical models based on physics and mechanics (Pudasaini, 2012; Pudasaini & Krautblatter, 2021; Pudasaini & Mergili, 2019) can not only reasonably explain experimental and field data but are also widely employed in numerical simulations of complex erosion processes, including catastrophic events (Liu et al., 2020; Mergili et al., 2020; Shugar et al., 2021). In the numerical inversion results of dam erosion in the glacial lake outbreak induced debris flow disaster simulated by Mergili et al. (2020), lateral erosion was underestimated, which may be attributed to slope instability not being fully considered. Periodic slope instability has been widely observed in the lateral erosion of this study and other related studies (Qin et al., 2018; Yan et al., 2020). However, the inversion results were consistent with the observed data overall, such as for the erosion volume (Mergili et al., 2020). This successful experience provided a valuable reference for the numerical simulation of the stored sediment erosion processes under the action of debris flow events after check dam removal. The results of this study may also provide references for numerical simulations from the perspective of not only the erosion volume but also the erosion distribution.

In the study of hydroelectric dam removal, previous studies have focused on the evolution of  $\lambda$  with time (Collins et al., 2017; Pearson et al., 2011), which is not suitable for debris flows because debris flows are different from streams and discontinuous in time (N. S. Chen et al., 2011; Imaizumi et al., 2019; Kean et al., 2013; Y. Li et al., 2013; Savage & Iverson, 2003). The evolution of  $\lambda$  with  $V_*$  (Equation 4) examined in this paper was more suitable for debris flows. As shown in Equation 4,  $\zeta$  was proportional to  $V_{\text{pote}}$  ( $\zeta = kV_{\text{pote}}$ ), which was obtained based on the experimental data of this study. Similar results were also noted in the field observations of hydroelectric dam removal (Collins et al., 2017; Pearson et al., 2011), but the values of  $k$  in these hydroelectric dam removal cases were much smaller than those in this study, which may be caused by the difference in  $C_v$  and  $Fr$  (Figure 8). In addition, according to the relationship between  $\zeta$  and erosion rate ( $\zeta = \overline{ES}/Q$ ), after making reasonable assumptions about the geomorphic characteristics of stored sediment, the value of  $k$  may also be obtained based on the calculation formulas of erosion rate (P. Li et al., 2020), erosion model (Iverson, 2012), and especially the mechanical erosion rate models (Pudasaini & Fischer, 2020; Pudasaini & Krautblatter, 2021). Stored sediment erosion is affected by multiple factors, such as the  $C_v$  of fluids,  $Fr$  of flows, grain size of stored sediment, and levels of cohesion and consolidation (Doyle et al., 2003; Ibisate et al., 2016; Ruan et al., 2021; Sawaske & Freyberg, 2012). More observations and experimental studies are needed to analyze the influencing factors, value of  $k$ , and the power of  $h_*$  to expand the application range of Equation 4. Equation 5 is the empirical expression of Equation 4 under the experimental conditions and may provide a reference for engineering practice similar to experimental conditions, such as debris flows with  $C_v = 0.18\text{--}0.30$ .

In terms of the method for removing check dams, this research mainly focused on the removed height. In addition to partial removal (Korpak & Lenar-Matyas, 2019), staged removal has been performed for many check dams (Ibisate et al., 2016), and in check dam groups, an investigation of the appropriate removal sequence was necessary (Collins et al., 2017). Further research on the staged removal and removal sequence of a dam group is of great significance to engineering practice. In summary, the geomorphological evolution of stored sediment after the removal of check dams and hydroelectric dams was similar. The main difference was in  $\zeta$  of debris flow and water flows, which may be caused by the difference in  $C_v$  and  $Fr$ . Equation 4 could effectively describe the evolution of the erosion volume, but more studies are necessary to determine the values of the relevant parameters and broaden its application range.

## 5. Conclusions

The influence of the removed height and debris flow surges on the stored sediment erosion processes after removing a check dam was investigated in this paper. Based on the experimental results, the following conclusions can be drawn:

1. The erosion processes of stored sediment could be divided into four stages: headward erosion initiation, incision and rill formation, lateral erosion and widening, and quasi-equilibrium. With the development of erosion, the erosion efficiency of debris flows gradually decreased. The erosion efficiency was positively correlated with the removed height, negatively correlated with the accumulated debris flow volume, and proportional to the remaining potential volume of sediment to be eroded.
2. The calculation formula of the erosion volume ratio, which was employed to characterize the erosion volume development process, was established:  $\lambda = h_*^2 (1 - \exp(-kV_*))$ , where  $h_*$  is the removed height ratio and  $V_*$  is the relative accumulated volume of the debris flow.  $k$  is a proportional coefficient denoting the ratio of the erosion efficiency to the remaining potential volume of sediment to be eroded and was approximately 0.54 and 0.66 for debris flows with sediment volume fractions of 0.18 and 0.30, respectively.
3. The distribution of eroded sediment along the longitudinal direction of the flume was described by the Weibull distribution. The scale parameter was negatively correlated with the removed height and positively correlated with the erosion volume ratio, and its empirical relationships were proposed. The shape parameter was mainly related to the removed height.

## Conflict of Interest

The authors declare no conflicts of interest relevant to this study.

## Data Availability Statement

The study data may be accessed at [https://zenodo.org/record/5562294#.YWQ\\_dWJByUk](https://zenodo.org/record/5562294#.YWQ_dWJByUk).

### Acknowledgments

This study was supported by the Second Tibetan Plateau Scientific Expedition and Research Program (Grant no. 2019QZKK0902), the National Natural Science Foundation of China (Grant no. 41925030), and the Chinese Academy of Sciences (CAS) Light of West China Program (Grant no. Y9R2140148).

### References

- Abbasi, N. A., Xu, X., Lucas-Borja, M. E., Dang, W., & Liu, B. (2019). The use of check dams in watershed management projects: Examples from around the world. *The Science of the Total Environment*, 676, 683–691. <https://doi.org/10.1016/j.scitotenv.2019.04.249>
- Cantelli, A., Paola, C., & Parker, G. (2004). Experiments on upstream-migrating erosional narrowing and widening of an incisional channel caused by dam removal. *Water Resources Research*, 40(3), W074361–W0743616. <https://doi.org/10.1029/2003WR002940>
- Chapuis, R. P. (2004). Predicting the saturated hydraulic conductivity of sand and gravel using effective diameter and void ratio. *Canadian Geotechnical Journal*, 41(5), 787–795. <https://doi.org/10.1139/t04-022>
- Chen, H. X., Li, J., Feng, S. J., Gao, H. Y., & Zhang, D. M. (2019). Simulation of interactions between debris flow and check dams on three-dimensional terrain. *Engineering Geology*, 251, 48–62. <https://doi.org/10.1016/j.enggeo.2019.02.001>
- Chen, J., Chen, X., Zhao, W., & You, Y. (2018). Debris flow drainage channel with energy dissipation structures: Experimental study and engineering application. *Journal of Hydraulic Engineering*, 144(10), 06018012. [https://doi.org/10.1061/\(ASCE\)HY.1943-7900.0001523](https://doi.org/10.1061/(ASCE)HY.1943-7900.0001523)
- Chen, J., Liu, W., Zhao, W., Jiang, T., Zhu, Z., & Chen, X. (2021). Magnitude amplification of flash floods caused by large woody in Jiuzhaigou National Park, China. *Geomatics. Natural Hazards and Risk*, 12(1), 2277–2299. <https://doi.org/10.1080/19475705.2021.1961882>
- Chen, J., Wang, D., Zhao, W., Chen, H., Wang, T., Nepal, N., & Chen, X. (2020). Laboratory study on the characteristics of large wood and debris flow processes at slit-check dams. *Landslides*, 17(7), 1703–1711. <https://doi.org/10.1007/s10346-020-01409-3>
- Chen, N., Yang, C., Zhou, W., Hu, G., Deng, M., & Yang, K. (2011). *Debris flow prospecting technology*. Beijing: Science Publisher.
- Chen, N. S., Yang, C. L., Zhou, W., Wei, F. Q., Li, Z. L., Han, D., & Hu, G. S. (2011). A new total volume model of debris flows with intermittent surges: Based on the observations at Jiangjia Valley, southwest China. *Natural Hazards*, 56(1), 37–57. <https://doi.org/10.1007/s11069-010-9548-z>
- Chen, X., Chen, J., Zhao, W., Li, Y., & You, Y. (2017). Characteristics of a debris-flow drainage channel with a step-pool configuration. *Journal of Hydraulic Engineering*, 143(9), 04017038. [https://doi.org/10.1061/\(asce\)hy.1943-7900.0001352](https://doi.org/10.1061/(asce)hy.1943-7900.0001352)
- Chen, X., Cui, P., You, Y., Chen, J., & Li, D. (2015). Engineering measures for debris flow hazard mitigation in the Wenchuan earthquake area. *Engineering Geology*, 194, 73–85. <https://doi.org/10.1016/j.enggeo.2014.10.002>
- Chen, Z., Huang, X., Yu, S., Cao, W., Dang, W., & Wang, Y. (2021). Risk analysis for clustered check dams due to heavy rainfall. *International Journal of Sediment Research*, 36(2), 291–305. <https://doi.org/10.1016/j.ijsrc.2020.06.001>
- Chiu, Y. F., Tfwala, S. S., Hsu, Y. C., Chiu, Y. Y., Lee, C. Y., & Chen, S. C. (2021). Upstream morphological effects of a sequential check dam adjustment process. *Earth Surface Processes and Landforms*, 46(13), 2527–2539. <https://doi.org/10.1002/esp.5178>
- Choi, C. E., Ng, C. W. W., Au-Yeung, S. C. H., & Goodwin, G. R. (2015). Froude characteristics of both dense granular and water flows in flume modelling. *Landslides*, 12(6), 1197–1206. <https://doi.org/10.1007/s10346-015-0628-8>
- Church, M., & Jakob, M. (2020). What is a debris flood? *Water Resources Research*, 56(8), e2020WR027144. <https://doi.org/10.1029/2020wr027144>
- Collins, M. J., Snyder, N. P., Boardman, G., Banks, W. S. L., Andrews, M., Baker, M. E., et al. (2017). Channel response to sediment release: Insights from a paired analysis of dam removal. *Earth Surface Processes and Landforms*, 42(11), 1636–1651. <https://doi.org/10.1002/esp.4108>
- Coussot, P., & Piau, J. M. (1994). On the behavior of fine mud suspensions. *Rheologica Acta*, 33(3), 175–184. <https://doi.org/10.1007/bf00437302>
- Cucchiari, S., Cavalli, M., Vericat, D., Crema, S., Llana, M., Beinat, A., et al. (2019). Geomorphic effectiveness of check dams in a debris-flow catchment using multi-temporal topographic surveys. *Catena*, 174, 73–83. <https://doi.org/10.1016/j.catena.2018.11.004>
- Cui, P., Zeng, C., & Lei, Y. (2015). Experimental analysis on the impact force of viscous debris flow. *Earth Surface Processes and Landforms*, 40(12), 1644–1655. <https://doi.org/10.1002/esp.3744>
- de Haas, T., Braat, L., Leuven, J. R. F. W., Lokhorst, I. R., & Kleinhans, M. G. (2015). Effects of debris flow composition on runout, depositional mechanisms, and deposit morphology in laboratory experiments. *Journal of Geophysical Research: Earth Surface*, 120(9), 1949–1972. <https://doi.org/10.1002/2015JF003525>
- Doyle, M. W., Stanley, E. H., & Harbor, J. M. (2003). Channel adjustments following two dam removals in Wisconsin. *Water Resources Research*, 39(1), 309–310. <https://doi.org/10.1029/2002WR001714>
- East, A. E., Logan, J. B., Mastin, M. C., Ritchie, A. C., Bountry, J. A., Magirl, C. S., & Sankey, J. B. (2018). Geomorphic evolution of a gravel-bed river under sediment-starved versus sediment-rich conditions: River response to the world's largest dam removal. *Journal of Geophysical Research: Earth Surface*, 123(12), 3338–3369. <https://doi.org/10.1029/2018JF004703>
- Fang, Q., Tang, C., Chen, Z., Wang, S., & Yang, T. (2019). A calculation method for predicting the runout volume of dam-break and non-dam-break debris flows in the Wenchuan earthquake area. *Geomorphology*, 327, 201–214. <https://doi.org/10.1016/j.geomorph.2018.10.023>
- Ferrer-Boix, C., Martín-Vide, J. P., & Parker, G. (2015). Channel evolution after dam removal in a poorly sorted sediment mixture: Experiments and numerical model. *Water Resources Research*, 50(11), 8997–9019. <https://doi.org/10.1002/2014WR015550>
- Fraccarollo, L., & Capart, H. (2002). Riemann wave description of erosional dam-break flows. *Journal of Fluid Mechanics*, 461, 183–228. <https://doi.org/10.1017/S0022112002008455>
- Galia, T., Škarpich, V., & Ruman, S. (2021). Impact of check dam series on coarse sediment connectivity. *Geomorphology*, 377, 107595. <https://doi.org/10.1016/j.geomorph.2021.107595>
- Grant, G. E. (1997). Critical flow constrains flow hydraulics in mobile-bed streams: A new hypothesis. *Water Resources Research*, 33(2), 349–358. <https://doi.org/10.1029/96wr03134>
- Haas, T. D., & Woerkm, T. V. (2016). Bed scour by debris flows: Experimental investigation of effects of debris-flow composition. *Earth Surface Processes and Landforms*, 41(13), 1951–1966. <https://doi.org/10.1002/esp.3963>
- Hong, Y., Wang, J. P., Li, D. Q., Cao, Z. J., Ng, C. W. W., & Cui, P. (2015). Statistical and probabilistic analyses of impact pressure and discharge of debris flow from 139 events during 1961 and 2000 at Jiangjia Ravine, China. *Engineering Geology*, 187, 122–134. <https://doi.org/10.1016/j.enggeo.2014.12.011>
- Huang, T., Ding, M., Gao, Z., & Tellez, R. D. (2021). Check dam storage capacity calculation based on high-resolution topogrammetry: Case study of the Cutou Gully, Wenchuan County, China. *The Science of the Total Environment*, 790, 148083. <https://doi.org/10.1016/j.scitotenv.2021.148083>

- Huebl, J., & Kaitna, R. (2021). Monitoring debris-flow surges and triggering rainfall at the Lattenbach Creek, Austria. *Environmental and Engineering Geoscience*, 27(2), 213–220. <https://doi.org/10.2113/EEG-D-20-00010>
- Hu, H., Zhou, G. G. D., Song, D., Cui, K. F. E., Huang, Y., Choi, C. E., & Chen, H. (2020). Effect of slit size on the impact load against debris-flow mitigation dams. *Engineering Geology*, 274, 105764. <https://doi.org/10.1016/j.enggeo.2020.105764>
- Ibisate, A., Ollero, A., Ballarín, D., Horacio, J., Mora, D., Mesanza, A., et al. (2016). Geomorphic monitoring and response to two dam removals: Rivers Urumea and Leizaran (Basque Country, Spain). *Earth Surface Processes and Landforms*, 41(15), 2239–2255. <https://doi.org/10.1002/esp.4023>
- Imaizumi, F., Masui, T., Yokota, Y., Tsunetaka, H., Hayakawa, Y., & Hotta, N. (2019). Initiation and runout characteristics of debris flow surges in Ohya landslide scar, Japan. *Geomorphology*, 339(5), 58–69. <https://doi.org/10.1016/j.geomorph.2019.04.026>
- Iverson, R. M. (1997). The physics of debris flows. *Reviews of Geophysics*, 35(3), 245–296. <https://doi.org/10.1029/97rg00426>
- Iverson, R. M. (2012). Elementary theory of bed-sediment entrainment by debris flows and avalanches. *Journal of Geophysical Research: Earth Surface*, 117(F3), F03006. <https://doi.org/10.1029/2011JF002189>
- Iverson, R. M. (2015). Scaling and design of landslide and debris-flow experiments. *Geomorphology*, 244, 9–20. <https://doi.org/10.1016/j.geomorph.2015.02.033>
- Kang, Z. C., Cui, P., Wei, F. Q., & He, S. F. (2007). *Observational experimental data set of the Dong Chuan Debris Flow Observation and Research Station of the Chinese Academy of Sciences (1995-2000)*. Beijing: Science Publisher.
- Kang, Z. C., Li, Z. F., Ma, A. N., & Luo, J. T. (2004). *Debris flow research in China*. Beijing: Science Publisher.
- Kean, J. W., McCoy, S. W., Tucker, G. E., Staley, D. M., & Coe, J. A. (2013). Runoff-generated debris flows: Observations and modeling of surge initiation, magnitude, and frequency. *Journal of Geophysical Research: Earth Surface*, 118(4), 2190–2207. <https://doi.org/10.1002/jgrf.20148>
- Korpak, J., & Lenar-Matyas, A. (2019). Stream channel changes as a result of sudden sediment release due to check dam lowering (Polish Carpathians). *Environmental Earth Sciences*, 78(14), 404. <https://doi.org/10.1007/s12665-019-8396-8>
- Li, P., Wang, J., Hu, K., & Wang, F. (2020). Experimental study of debris-flow entrainment over stepped-gradient beds incorporating bed sediment porosity. *Engineering Geology*, 274, 105708. <https://doi.org/10.1016/j.enggeo.2020.105708>
- Li, S., You, Y., Chen, X., Liu, J., & Chen, J. (2019). Regulation effectiveness of a window-check dam on debris flows. *Engineering Geology*, 253, 205–213. <https://doi.org/10.1016/j.enggeo.2019.03.020>
- Li, Y., Zhou, X., Su, P., Kong, Y., & Liu, J. (2013). A scaling distribution for grain composition of debris flow. *Geomorphology*, 192, 30–42. <https://doi.org/10.1016/j.geomorph.2013.03.015>
- Liu, W., Yan, S., & He, S. (2020). A simple method to evaluate the performance of an intercept dam for debris-flow mitigation. *Engineering Geology*, 276, 105771. <https://doi.org/10.1016/j.enggeo.2020.105771>
- Lucas-Borja, M. E., Piton, G., Yu, Y., Castillo, C., & Antonio Zema, D. (2021). Check dams worldwide: Objectives, functions, effectiveness and undesired effects. *Catena*, 204, 105390. <https://doi.org/10.1016/j.catena.2021.105390>
- Major, J. J., Spicer, K. R., Rhode, A., O'Connor, J. E., Bragg, H. M., Tanner, D. Q., et al. (2008). Initial fluvial response to the removal of Oregon's Marmot Dam. *Eos, Transactions American Geophysical Union*, 89(27), 241–242. <https://doi.org/10.1029/2008eo270001>
- Meng, X. (2012). Landslides & debris flows in Southern Gansu, China and formation of the catastrophic Zhouqu debris flow disaster in August 2010. *Quaternary International*, 279–280, 322–323. <https://doi.org/10.1016/j.quaint.2012.08.918>
- Mergili, M., Fischer, J. T., Krenn, J., & Pudasaini, S. P. (2017). r.avaflow v1, an advanced open-source computational framework for the propagation and interaction of two-phase mass flows. *Geoscientific Model Development*, 10(2), 553–569. <https://doi.org/10.5194/gmd-10-553-2017>
- Mergili, M., Pudasaini, S. P., Emmer, A., Fischer, J. T., Cochachin, A., & Frey, H. (2020). Reconstruction of the 1941 GLOF process chain at Lake Palcacocha (Cordillera Blanca, Peru). *Hydrology and Earth System Sciences*, 24(1), 93–114. <https://doi.org/10.5194/hess-24-93-2020>
- Mikoš, M., Kryžanowski, A., Martinčič, M., & Sodnik, J. (2014). Concrete torrent check-dams and debris-flow magnitudes. In K. Sassa, P. Canuti, & Y. Yin (Eds.), *Landslide science for a safer geoenvironment* (pp. 51–56). Cham: Springer International Publishing.
- Mooney, M. (1951). The viscosity of a concentrated suspension of spherical particles. *Journal of Colloid Science*, 6(2), 162–170. [https://doi.org/10.1016/0095-8522\(51\)90036-0](https://doi.org/10.1016/0095-8522(51)90036-0)
- Pan, H., Wang, R., Huang, J., & Ou, G. (2013). Study on the ultimate depth of scour pit downstream of debris flow sabo dam based on the energy method. *Engineering Geology*, 160, 103–109. <https://doi.org/10.1016/j.enggeo.2013.03.026>
- Pearson, A. J., Snyder, N. P., & Collins, M. J. (2011). Rates and processes of channel response to dam removal with a sand-filled impoundment. *Water Resources Research*, 47(8), W08504. <https://doi.org/10.1029/2010wr009733>
- Piton, G., & Recking, A. (2016). Design of sediment traps with open check dams. I: Hydraulic and deposition processes. *Journal of Hydraulic Engineering*, 142(2), 04015045. [https://doi.org/10.1061/\(ASCE\)HY.1943-7900.0001048](https://doi.org/10.1061/(ASCE)HY.1943-7900.0001048)
- Pourghasemi, H. R., Yousefi, S., Sadhasivam, N., & Eskandari, S. (2020). Assessing, mapping, and optimizing the locations of sediment control check dams construction. *The Science of the Total Environment*, 739, 139954. <https://doi.org/10.1016/j.scitotenv.2020.139954>
- Pudasaini, S. P. (2012). A general two-phase debris flow model. *Journal of Geophysical Research: Earth Surface*, 117, F03010. <https://doi.org/10.1029/2011JF002186>
- Pudasaini, S. P., & Fischer, J. T. (2020). A mechanical erosion model for two-phase mass flows. *International Journal of Multiphase Flow*, 132, 103416. <https://doi.org/10.1016/j.ijmultiphaseflow.2020.103416>
- Pudasaini, S. P., & Krautblatter, M. (2021). The mechanics of landslide mobility with erosion. *Nature Communications*, 12, 6793. <https://doi.org/10.1038/s41467-021-26959-5>
- Pudasaini, S. P., & Kröner, C. (2008). Shock waves in rapid flows of dense granular materials: Theoretical predictions and experimental results. *Physical Review E, Statistical, Nonlinear, and Soft Matter Physics*, 78(4 Pt 1), 041308. <https://doi.org/10.1103/PhysRevE.78.041308>
- Pudasaini, S. P., & Mergili, M. (2019). A multi-phase mass flow model. *Journal of Geophysical Research: Earth Surface*, 124(12), 2920–2942. <https://doi.org/10.1029/2019JF005204>
- Qin, C., Zheng, F., Wells, R. R., Xu, X., Wang, B., & Zhong, K. (2018). A laboratory study of channel sidewall expansion in upland concentrated flows. *Soil and Tillage Research*, 178, 22–31. <https://doi.org/10.1016/j.still.2017.12.008>
- Randle, T. J., Bountry, J. A., Ritchie, A., & Wille, K. (2015). Large-scale dam removal on the Elwha River, Washington, USA: Erosion of reservoir sediment. *Geomorphology*, 246, 709–728. <https://doi.org/10.1016/j.geomorph.2014.12.045>
- Rickenmann, D. (1999). Empirical relationships for debris flows. *Natural Hazards*, 19(1), 47–77. <https://doi.org/10.1023/A:1008064220727>
- Ruan, H., Chen, H., Li, Y., Chen, J., & Li, H. (2021). Study on the downcutting rate of a debris flow dam based on grain-size distribution. *Geomorphology*, 391, 107891. <https://doi.org/10.1016/j.geomorph.2021.107891>
- Savage, S. B., & Iverson, R. M. (2003). Surge dynamics coupled to pore-pressure evolution in debris flows. *Paper presented at the International Conference on Debris-Flow Hazards Mitigation: Mechanics, Prediction, and Assessment*. Switzerland: Davos.
- Sawaske, S. R., & Freyberg, D. L. (2012). A comparison of past small dam removals in highly sediment-impacted systems in the U.S. *Geomorphology*, 151–152, 50–58. <https://doi.org/10.1016/j.geomorph.2012.01.013>

- Shima, J., Moriyama, H., Kokuryo, H., Ishikawa, N., & Mizuyama, T. (2016). Prevention and mitigation of debris flow hazards by using steel open-type sabo dams. *International Journal of Erosion Control Engineering*, 9, 135–144. <https://doi.org/10.13101/ijece.9.135>
- Shugar, D. H., Jacquemart, M., Shean, D., Bhushan, S., Upadhyay, K., Sattar, A., et al. (2021). A massive rock and ice avalanche caused the 2021 disaster at Chamoli, Indian Himalaya. *Science*, 373(6552), 300–306. <https://doi.org/10.1126/science.abh4455>
- Sodnik, J., Martinčič, M., Mikoš, M., & Kryżanowski, A. (2015). Are torrent check-dams potential debris-flow sources? In G. Lollino, D. Giordan, G. B. Crosta, J. Corominas, R. Azzam, J. Wasowski, & N. Sciarra (Eds.), *Engineering geology for society and territory*. (Vol. 2, pp. 485–488). Cham: Springer International Publishing. [https://doi.org/10.1007/978-3-319-09057-3\\_79](https://doi.org/10.1007/978-3-319-09057-3_79)
- Song, D., Zhou, G. G., Chen, X. Q., Li, J., Wang, A., Peng, P., & Xue, K. X. (2021). General equations for landslide-debris impact and their application to debris-flow flexible barrier. *Engineering Geology*, 288, 106154. <https://doi.org/10.1016/j.enggeo.2021.106154>
- Tseng, W. H., Wang, H. W., Chou, S. C., Kao, Y. L., & Shieh, C. L. (2012). Experiments on channel evolution caused by check-dam failure. *Journal of Mountain Science*, 9(2), 175–184. <https://doi.org/10.1007/s11629-012-2252-6>
- Wang, G. L. (2013). Lessons learned from protective measures associated with the 2010 Zhouqu debris flow disaster in China. *Natural Hazards*, 69(3), 1835–1847. <https://doi.org/10.1007/s11069-013-0772-1>
- Wang, H. W., Cheng, Y. C., & Lin, C. Y. (2014). Experiments on channel evolution due to dam removal in Taiwan. *Journal of Mountain Science*, 11(6), 1396–1405. <https://doi.org/10.1007/s11629-014-3088-z>
- Wang, H. W., & Kuo, W. C. (2016). Geomorphic responses to a large check-dam removal on a mountain river in Taiwan. *River Research and Applications*, 32(5), 1094–1105. <https://doi.org/10.1002/rra.2929>
- Wang, Z., Chen, Z., Yu, S., Zhang, Q., Wang, Y., & Hao, J. (2021). Erosion-control mechanism of sediment check dams on the Loess Plateau. *International Journal of Sediment Research*, 141, 668–677. <https://doi.org/10.1016/j.ijsrc.2021.02.002>
- Warrick, J. A., Bountry, J. A., East, A. E., Magirl, C. S., Randle, T. J., Gelfenbaum, G., et al. (2015). Large-scale dam removal on the Elwha River, Washington, USA: Source-to-sink sediment budget and synthesis. *Geomorphology*, 246, 729–750. <https://doi.org/10.1016/j.geomorph.2015.01.010>
- White, S., García-Ruiz, J. M., Martí, C., Valero, B., Errea, M. P., & Gómez-Villar, A. (1997). The 1996 Biescas campsite disaster in the Central Spanish Pyrenees, and its temporal and spatial context. *Hydrological Processes*, 11(14), 1797–1812. [https://doi.org/10.1002/\(SICI\)1099-1085\(199711\)11:14<1797::AID-HYP605>3.0.CO;2-7](https://doi.org/10.1002/(SICI)1099-1085(199711)11:14<1797::AID-HYP605>3.0.CO;2-7)
- Yan, H., Ge, Y., Guo, X., Zhan, M., & Du, Y. (2020). The randomness of lateral erosion failure of debris flow gully deposits. *Journal of Natural Disasters*, 29(6), 85–97.
- Yang, H. J., Hu, K. H., & Wei, F. Q. (2013). Methods for computing rheological parameters of debris-flow slurry and their extensibilities. *Journal of Hydraulic Engineering*, 44(11), 1338–1346.
- Yu, B., Ma, Y., & Wu, Y. (2013). Case study of a giant debris flow in the Wenjia Gully, Sichuan Province, China. *Natural Hazards*, 65(1), 835–849. <https://doi.org/10.1007/s11069-012-0395-y>
- Zanuttigh, B., & Lamberti, A. (2007). Instability and surge development in debris flows. *Reviews of Geophysics*, 45(3). <https://doi.org/10.1029/2005rg000175>
- Zhang, F., Yan, B., Feng, X., Lan, H., Kang, C., Lin, X., et al. (2019). A rapid loess mudflow triggered by the check dam failure in a bulldozer mountain area, Lanzhou, China. *Landslides*, 16(10), 1981–1992. <https://doi.org/10.1007/s10346-019-01219-2>
- Zhang, J., & Xiong, G. (1997). *Data collection of kinematic observation of debris flows in Jiangjia Ravine, Dongchuan, Yunnan*. Beijing: Science Publisher.
- Zhang, X., She, D., Hou, M., Wang, G., & Liu, Y. (2021). Understanding the influencing factors (precipitation variation, land use changes and check dams) and mechanisms controlling changes in the sediment load of a typical Loess watershed, China. *Ecological Engineering*, 163, 106198. <https://doi.org/10.1016/j.ecoleng.2021.106198>
- Zhou, G. G. D., Hu, H. S., Song, D., Zhao, T., & Chen, X. Q. (2019). Experimental study on the regulation function of slit dam against debris flows. *Landslides*, 16(1), 75–90. <https://doi.org/10.1007/s10346-018-1065-2>
- Zhu, X. H., Cui, P., Chen, H. Y., & Tang, J. B. (2013). Research on the mechanism of failure and sediment delivery of landslide dams in debris flow channel. In K. Ugai, H. Yagi, & A. Wakai (Eds.), *Earthquake-induced landslides* (pp. 907–915). Berlin, Heidelberg: Springer.